Huge Reduction of the Wake-Up Effect in Ferroelectric HZO Thin Films

Jordan Bouaziz, Pedro Rojo Romeo, Nicolas Baboux, Bertrand Vilquin

ACS APPLIED ELECTRONIC MATERIALS

Letter

pubs.acs.org/acsaelm

Huge Reduction of the Wake-Up Effect in Ferroelectric HZO Thin Films

Jordan Bouaziz,*[,†,‡] Pedro Rojo Romeo,[†] Nicolas Baboux,[‡] and Bertrand Vilquin[†]

[†]Université de Lyon, Institut des Nanotechnologies de Lyon (UMR5270/CNRS), Ecole Centrale de Lyon, 36 avenue Guy de Collongue, F-69134 Ecully Cedex, France

[‡]Université de Lyon, Institut des Nanotechnologies de Lyon (UMR5270/CNRS), INSA, Bât. Blaise Pascal, 7 avenue Jean Capelle, F-69621 Villeurbanne Cedex, France

Supporting Information

ABSTRACT: The wake-up effect is a major issue for ferroelectric HfO_2-based memory devices. Here, two TiN/HZO/TiN structures deposited by magnetron sputtering on silicon are compared. The maximum remanant polarization is higher than 21 $\mu C/cm^2$ for both samples, but a strong difference is observed in the electrical behavior. For the mesa sample, the difference between the maximum and initial remanent polarization is only 3 $\mu C/cm^2$, whereas it is around 14 $\mu C/cm^2$ in the non-mesa case. We discuss the root causes of these behaviors in light of GIXRD results.

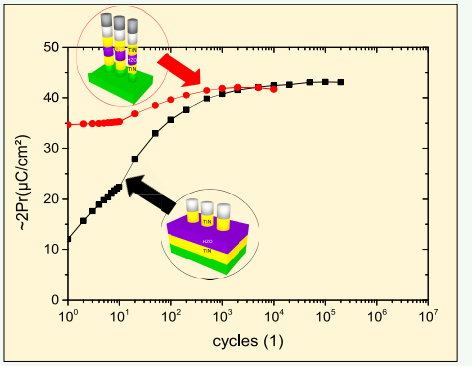

KEYWORDS: *HfO_2, ZrO_2, HZO, ferroelectricity, wake-up effect, FRAM*

The discovery of ferroelectric Si-doped HfO_2[1] has paved the way to a wide variety of research interests and technical developments. The growing number of papers dealing with HfO_2-based materials[2] is a relevant indicator of the growing interest for this subject. Undeniably, many applications could benefit from ferroelectric HfO_2-based materials such as ferroelectric random access memory (FRAM), a ferroelectric field effect transistor (FeFET), a negative capacitance field effect transistor (NCFET), a ferroelectric tunnel junction (FTJ), synaptic devices, pyroelectric energy harvesters, piezoelectric devices, and so on. However, major issues are still hindering the appearance of ferroelectric HfO_2-based materials on the market. These issues are mainly related to the well-known wake-up effect, imprint, fatigue, and endurance. Recent studies on the subject point out crystallographic phase change and oxygen vacancy diffusion during cycling as the root causes of the issues cited above.

Of all the numerous dopants that have been tested in ferroelectric HfO_2-based materials, the most addressed is probably Zr^{4+}, because both HfO_2 and ZrO_2 are already used in the CMOS[3] and DRAM[4] industries. Moreover, Zr^{4+} allows the lowest annealing temperature of all dopants, making it compatible with the silicon semiconductor industry.

Compared to the hundreds of articles dealing with (Hf, Zr)O_2 solid solutions (HZO) deposited by ALD, sputtering has rarely been used.[5−14] However, the deposition of materials by sputtering shows many benefits compared to ALD:

(i) Sputtering can be much faster than ALD deposition.
(ii) Sputtering can prevent carbon contamination that cannot be avoided with ALD precursors.
(iii) The deposition can be performed at room temperature.
(iv) In principle, sputtering can be carried out in one run in the same sputtering chamber.
(v) Sputtering is a low-cost reproducible process.

Consequently, HZO development could be greatly enhanced by using sputtering.

Moreover, most of the articles dealing with HZO sputtering use cosputtering.[7−9,11,13,14] Cosputtering enables more parameters to be tuned, particularly the Zr doping.[11] However, for industrial manufacturing, single target sputtering appears to be simpler and less expensive.

In this work, two different structures were realized by magnetron sputtering with a single target. Their performances are among the best in sputtering, but their behaviors are completely different. Particularly, the mesa structure presents a significantly reduced wake-up effect. We discuss the origins of these differences and the consequences for electrical measurement methods used to characterize ferroelectric HfO_2-based materials.

The structure shown in Figure 1a is called NM-sample for "non-mesa" structure and the structure shown in Figure 1b is called M-sample for "mesa" structure.

Received: June 11, 2019
Accepted: August 23, 2019
Published: August 23, 2019

DOI: 10.1021/acsaelm.9b00367
ACS Appl. Electron. Mater. XXXX, XXX, XXX−XXX

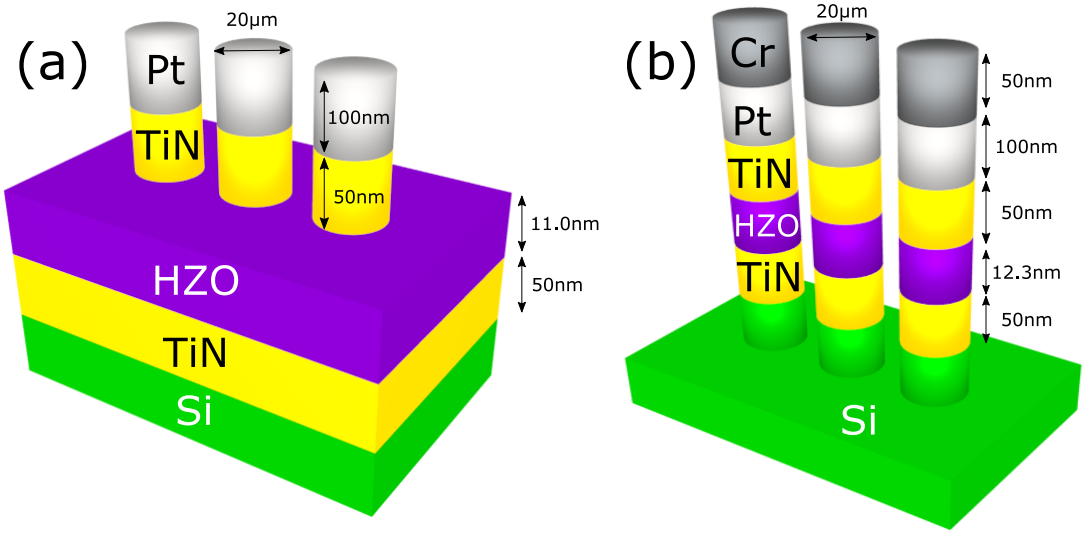

Figure 1. Scheme of (a) the NM-sample and (b) M-sample.

Si substrates were cleaned with ultrasonication in acetone and ethanol for 1 min. Substrates are Si-doped and (100)-oriented. The native oxide layer of each substrate is removed by a buffer oxide etch (BOE) process. For both processes, a 50 nm-thick bottom electrode (BE) is deposited in the conditions detailed in Table 1. This layer blankets the entire Si substrate.

Table 1. Film Growth Conditions for TiN and HZO

	sputtering	
target−substrate distance	8 cm	
base pressure	$<5 \times 1^{-7}$ mbar	
deposited elements	TiN	$(Hf, Zr)O_2$
substrate	Si	Si/TiN
target	Ti	ZrO_2/HfO_2 (50/50)
target RF power	300 W	100 W
holder DC bias voltage	60 V	none
gas	Ar = 50 sccm	Ar = 50 sccm
	N_2 = 3 sccm	
working pressure	5×10^{-3} mbar	5×10^{-2} mbar
deposition speed	5.2 nm/min	5 nm/min
rapid thermal annealing (RTA) conditions		
temperature	450 °C	
atmosphere	N_2	
duration	30 s	

Then, an HZO layer covering the whole TiN layer is deposited. The HZO thickness is measured by X-ray reflectivity (XRR). HZO layers are 12.3 nm-thick and 11.0 nm-thick for the M-sample and the NM-sample, respectively.

For the NM-sample, UV photolithography is carried out. Then, a 50 nm-thick TiN TE followed by a 100 nm Pt top electrode for mechanical and electrical contact are deposited. A lift-off step is then performed. Finally, the NM-sample is annealed by RTA under the conditions described in Table 1. It means that, for the NM-sample, HZO is only partially covered during the RTA crystallization process.

For the M-sample, the HZO layer is blanketed with a 50 nm-thick TiN layer. Then, UV photolithography and lift-off are carried out to define the electrodes with the deposition of a 100 nm-thick Pt layer followed by a 50 nm-thick Cr layer. Cr is used as a hard mask for etching. The M-sample is annealed by RTA in the conditions described in Table 1. Finally, the sample is etched by RIE at 300 W (RF) for 20 min with SF_6 as a reactive gas. The final structure is presented in Figure 1b. For this structure, HZO is fully covered with TiN TE during the annealing step.

GIXRD is performed on a four-circle Smartlab Rigaku diffractometer using a 9 kW copper rotating anode.

Electrical characterization is carried out on 20 μm diameter capacitors using a probe station and a setup composed of an arbitrary waveform generator (Nippon Factory WF1966), a transimpedance current amplifier (Keithley 428), and a 12 bit Digital Storage Oscilloscope (Nicolet Integra 40).

Endurance tests were performed with bipolar square pulses (commonly called set/reset sequence) until breakdown. The set/reset sequence is achieved in two different configurations: 2.5 kHz/3.5 V and 1.0 MHz/3.0 V. The first sequence allows the stress to be maximized without breakdown. The second set/reset sequence is used in order to be as close as possible to the microelectronic standard, and it is therefore used as a reference.

P−*E* curves are obtained using the PUND technique. This consists of applying a negative set pulse followed by two positive pulses (P and U) and then two negative pulses (N and D). The PUND maximum amplitude voltage equals that of the set/reset sequence. PUND pulses are triangular pulses with a rise/fall time of 100 μs, corresponding to 2.5 kHz $\left(= \frac{1}{4 \times 100}\ \mu s^{-1} \right)$.

First, the change of the sum of the absolute values of the positive remanent polarization and the negative remanent polarization $|P_{r+}| + |P_{r-}|$ during cycling is studied. Figure 2 shows the results for the two different set/reset sequences described in the experimental section.

At 1.0 MHz and 3.0 V (Figure 2a), $|P_{r+}| + |P_{r-}|$ for the NM-sample starts at around 5 $\mu C/cm^2$. This value increases until 10^5 cycles, where it reaches around 29 $\mu C/cm^2$. Then, it decreases until breakdown. Such an effect is not observable for the M-sample. Indeed, $|P_{r+}| + |P_{r-}|$ starts at 25 $\mu C/cm^2$ (instead of 5 $\mu C/cm^2$ for the NM-sample) and reaches a maximum of 32.8 $\mu C/cm^2$ at 2×10^3 cycles. So, the wake-up effect can be considered negligible in these conditions. Subsequently, fatigue

DOI: 10.1021/acsaelm.9b00367
ACS Appl. Electron. Mater. XXXX, XXX, XXX−XXX

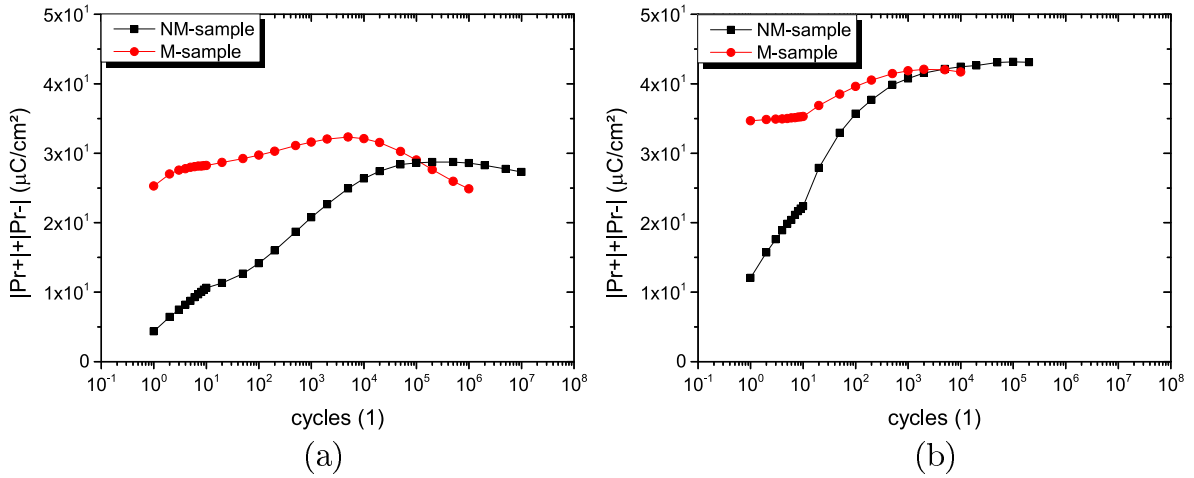

Figure 2. Change of $|P_{r+}| + |P_{r-}|$ versus the number of cycles with the stress conditions (a) 1.0 MHz and 3.0 V and (b) 2.5 kHz and 3.5 V for the NM-sample (black curve) and M-sample (red curve).

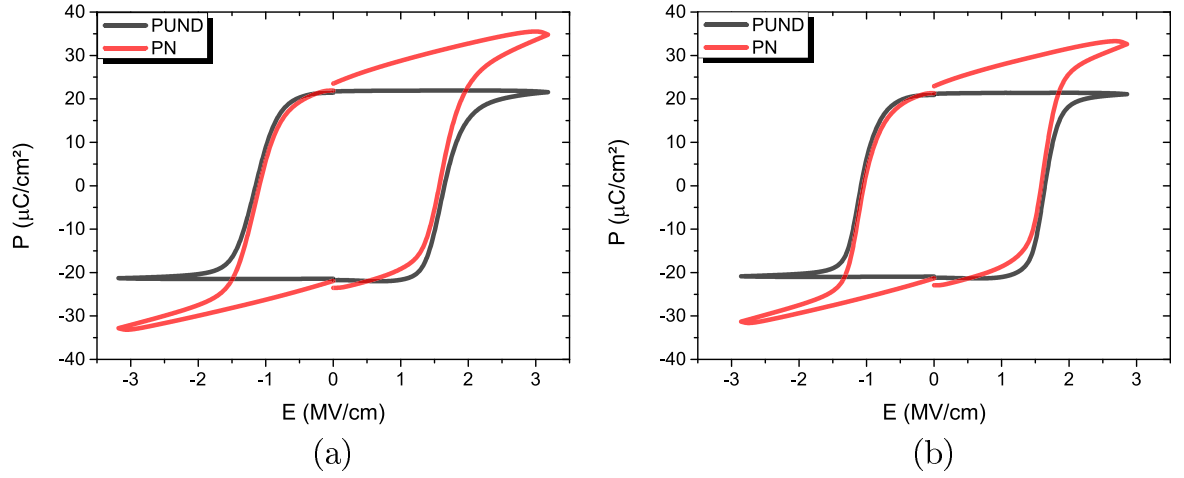

Figure 3. Polarization versus applied electrical field for (a) the NM-sample at 10^5 cycles and (b) the M-sample at 2×10^3 cycles under the stress conditions: 2.5 kHz and 3.5 V.

begins and breakdown occurs after 5×10^5 cycles. In comparison, the NM-sample breaks down after 1×10^7 cycles.

More severe stress conditions were also applied (Figure 2b). The same tendencies are observed: here, the wake-up effect is also significantly reduced on the M-sample compared to that on the NM-sample, but it is detrimental for the endurance of the M-sample. In fact, the breakdown occurs at a lower number of cycles for the M-sample compared to for the NM-sample.

For both samples, $|P_{r+}| + |P_{r-}|$ values are much higher at 2.5 kHz/3.5 V and the breakdown occurs earlier. These results are consistent with previous observations.[15−17]

For both stress conditions, the P_r of the NM-sample increases until it exceeds the P_r of the M-sample for a given number of cycles, because fatigue occurs earlier for the M-sample. As a consequence, at 1.0 MHz/3.0 V (Figure 3a), between the first cycle and the breakdown, the M-sample has a higher maximum P_r = 16.4 μC/cm ^{2} than the NM-sample, whereas at 2.5 kHz/3.5 V (Figure 2b), the M-sample has a higher maximum P_r = 21.7 μC/cm ^{2}. This is due to the reduced wake-up effect. In fact, with the M-sample, the maximum remanent polarization is always reached very rapidly, whereas with the NM-sample, the higher the stress conditions, the faster you can reach the maximum remanent polarization. Moreover, for the NM-sample, fatigue is always reached at around 10^6 cycles, which means that under a low-stress sequence, fatigue is reached on the NM-sample before crossing the curve of the M-sample. It follows that the M-sample has a higher remanent polarization under low-stress conditions, whereas the NM-sample has a higher maximum remanent polarization under high-stress conditions. Therefore, the maximum P_r seems to be more dependent on the stress conditions than on the structures themselves, which could have important consequences on industrial applications.

The M-sample has a reduced wake-up effect, but it also shows a sign of fatigue before the NM-sample. It is possible that the M-sample is already in an awake state, which leads to the absence of wake-up and an earlier fatigue and breakdown compared to the NM-sample.

For the M-sample, the maximum P_r minus the initial P_r is around 3−4 μC/cm^2 in both conditions. In comparison, the difference is between 12 and 16 μC/cm^2 for the NM-sample. There is 1 order of magnitude between both increases of P_r during the wake-up.

In high-stress conditions, there is no double peak for the M-sample, and in low-stress conditions, the double peak disappears at the second measurement cycle. For the NM-

DOI: 10.1021/acsaelm.9b00367
ACS Appl. Electron. Mater. XXXX, XXX, XXX−XXX

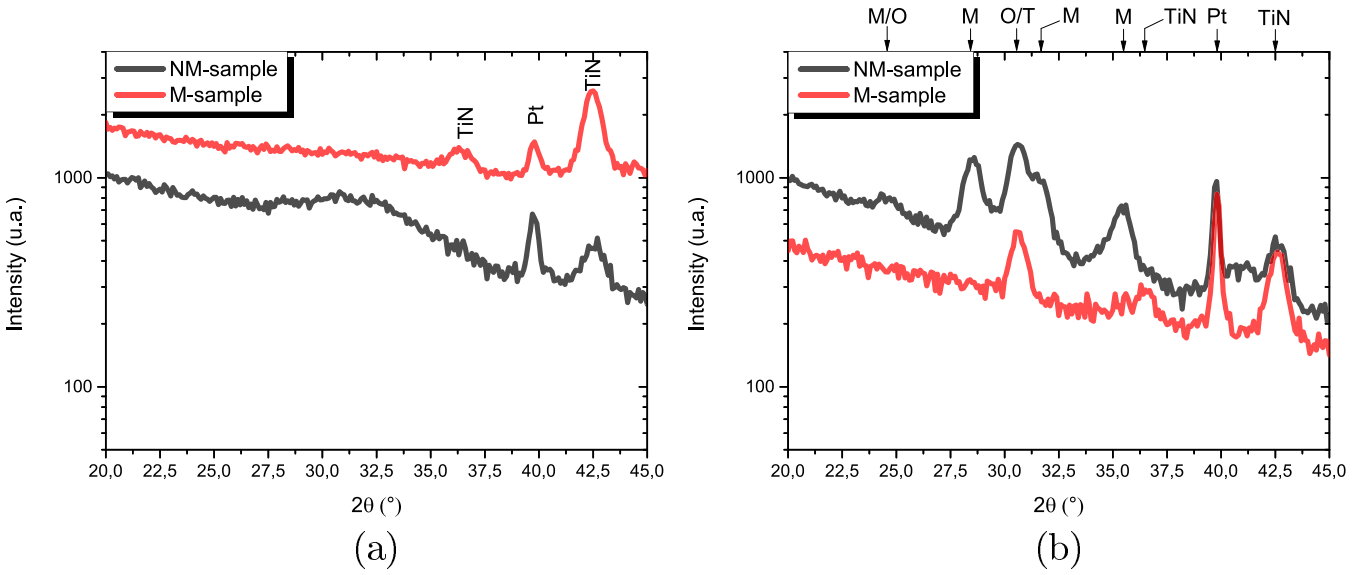

Figure 4. GIXRD measurements comparing the NM-sample (black curve) and the M-sample (red curve) (a) before RTA and (b) after RTA. M stands for monoclinic, O stands for orthorhombic, and T stands for tetragonal phases.

sample, a double peak is clearly observable during the first measurement cycle, and a small peak (coming from the double peak) is observable until 10^3 cycles for high-stress conditions and until 5×10^4 cycles for low-stress conditions (see the Supporting Information for more details).

Finally, at 10 cycles, an inflection point can be seen. It is caused by the measurements realized due to the PUND technique, which also wakes the sample. The PUND measurement is negligible after 20 cycles, as compared to the set/reset cycles.

It is to be noted that these results have been reproduced on many electrodes.

To assess the quality of our films, Figure 3 shows the polarization versus the electrical field when P_r has reached its maximum value. PUND and PN curves are represented. The value of P_r is higher in PN curves, because PN includes the leakage current. P_r values of the PN measurements have not been discussed in this report, because they can include extrinsic effects. Leakage is very well-compensated, because the PN curves show open cycles, whereas PUND does not. Also, the $P-E$ curves by PUND show very pinched cycles, which means that the samples are very well-saturated.

Then, grazing incidence X-ray diffraction is carried out to enlighten the electrical characterizations. Figure 4 shows GIXRD results before (Figure 4a) and after (Figure 4b) annealing of the NM-sample and the M-sample. ICDD card nos. 00-038-1420 and 00-004-0802 were respectively used for TiN and Pt. For the HZO m-phase, ICDD card no. 04-002-5428 was used. The peak at around 30.5° for the o/t-phase came from the work of Lee et al.,[8] and we knew from the first paper on ferroelectricity in hafnium oxide by Böscke et al.[1] that a peak at around 25° can be mistaken with the peak coming from the m-phase at this angle. In Figure 4a, the M-sample presents a TiN(111) peak, which is not visible in the NM-sample. This is probably caused by the different structures of the TiN TE in each sample. Comparing the NM-sample and the M-sample in Figure 4b, it is clear that the polycrystalline nature of the samples is completely different. The NM-sample shows clear monoclinic phases (m-phases), whereas no monoclinic peak can be seen in the M-sample. On the M-sample, only the o(111) peak can be seen. Other peaks come from the electrodes.

At the microcrystalline scale, the orthorhombic phase (o-phase) is recognized as the origin of ferroelectricity. m-Phases are assumed to be parasitic phases for ferroelectricity. Two hypotheses are generally considered as the causes of the wake-up effect according to Fengler et al:[18] crystallographic phase change contributions and oxygen vacancy diffusion. Grimley et al.[19] have observed a phase transition from the m- to the o-phase using scanning transmission electron microscopy (STEM) and impedance spectroscopy. Therefore, tremendous reduction in the amount of m-phase in the M-sample could have led to a drastic decrease in the wake-up effect. Moreover, the presence of many monoclinic orientations coexisting with the o-phase on the NM-sample could also play a key role in the oxygen vacancy redistribution, because the number of interfaces between crystallites has increased on the NM-sample. In fact, the crystalline structure influences the redistribution of charged defects, the mobility of these charges, charge trapping, and charge screening. For that reason, it can be concluded that the microcrystalline structure seems to be the main parameter influencing the two different electrical behaviors observed in this Letter.

One could argue that the different crystalline structures are due to the TiN TE difference between the two samples. In fact, in the case of the M-sample, TiN is blanketed over the entire HZO layer, whereas in the case of the NM-sample, it covers only the areas under the top electrodes. This implies a completely different stress state between the two samples. As a consequence, in the case of the M-sample, it turns the o-phase into the lowest energy phase. It has actually been demonstrated that TiN TE acts as a tensile stressor on the HZO film during the annealing process.[20−24] The stress inhibits the formation of the monoclinic phase during HZO crystallization, forming an orthorhombic phase that generates a large ferroelectric polarization, even at low process temperatures.

Finally, Chernikova et al.[25] compare the P_r performances of an HZO layer and a La-doped HZO layer called "HZLO". The HZO layer has a very low wake-up effect but also a very low endurance, whereas HZLO has a very high endurance with a

DOI: 10.1021/acsaelm.9b00367
ACS Appl. Electron. Mater. XXXX, XXX, XXX−XXX

very high wake-up effect. The exact same phenomenon is observed here when measuring the NM-sample and the M-sample. Consequently, the root causes of the huge reduction of the wake-up effect and the decreasing of cycles before breakdown in both articles could be assumed to be the same. However, they observed that "the HZLO film showed a slightly larger grain size compared to the HZO film". Consequently, according the authors of the article, "the bulk free energy difference between the FE o-phase and non-FE m-phase decreased after La doping." Unfortunately, this cannot explain what is happening in our work, because the observation of clear monoclinic peaks in the GIXRD pattern of the NM-sample Figure 4b suggests that the free energy difference decreases. Manufacturing both structures with HZLO instead of HZO may help to shed light on this mystery.

This Letter reports the fabrication of two samples deposited by magnetron sputtering with excellent performances, quite similar to samples deposited by ALD.[25] P_r values are among the highest for samples deposited by sputtering.

Although the M-sample and the NM-sample show very similar maximum P_r values, both samples demonstrate completely different electrical behavior. During cycling, the increase of the P_r value for the NM-sample is more than an order of magnitude higher than that of the M-sample. It is accompanied by a decrease of the endurance, which is 2 orders of magnitude higher for the NM-sample than for the M-sample.

As the electrical behaviors are not the same, for low-stress conditions, the M-sample has a higher maximum P_r value during cycling, whereas for high-stress conditions, the NM-sample has a higher P_r value during cycling. As a matter of fact, it has been proven that maximum P_r values are more sensitive to stress conditions than the to structures themselves.

The origins of the different electrical behaviors come from the microcrystalline structures of the two samples, according to GIXRD results. The crystallization takes place during the annealing step. During annealing, the M-sample is built with a TiN TE fully covering the HZO layer, whereas the TiN only partially covers the HZO layer in the case of the NM-sample. It induces different stress states, which lead to two different microcrystalline patterning. The M-sample shows no monoclinic peak, whereas the NM-sample shows many monoclinic orientations. This explains the huge reduction of the wake-up effect.

■ ASSOCIATED CONTENT

Supporting Information

The Supporting Information is available free of charge on the ACS Publications website at DOI: 10.1021/acsaelm.9b00367.

Chronograms for the M-sample and NM-sample describing the presence, the absence, and the mergers of the double peak obtained due to the PUND measurements (PDF)

■ AUTHOR INFORMATION

Corresponding Author

*E-mail: jordan.bouaziz@insa-lyon.fr.

ORCID

Jordan Bouaziz: 0000-0003-0975-5066

Notes

The authors declare no competing financial interest.

■ ACKNOWLEDGMENTS

This work was realized on the NanoLyon technology platform and has received funding from the European Union's Horizon 2020 Research and Innovation Programme under grant agreement n° 780302. We also thank GDR OxyFun for its financial support. We also thank Ruben Vera, Erwann Jeanneau (Centre de Diffractométrie Henri Longchambon, Université de Lyon), and Ingrid Cañero Infante (Institut des Nanotechnologies de Lyon) for their help in the XRD data analysis.

■ REFERENCES

(1) Böscke, T. S.; Müller, J.; Bräuhaus, D.; Schröder, U.; Böttger, U. Ferroelectricity in Hafnium Oxide Thin Films. *Appl. Phys. Lett.* **2011**, *99*, 102903.

(2) Park, M. H.; Lee, Y. H.; Mikolajick, T.; Schroeder, U.; Hwang, C. S. Review and Perspective on Ferroelectric HfO_2-based Thin Films for Memory Applications. *MRC* **2018**, *8*, 795−808.

(3) Kim, K. From the Future Si Technology Perspective: Challenges and Opportunities. *2010 IEEE International Electron Devices Meeting (IEDM)* **2010**, 1.1.1−1.1.9.

(4) James, D. Recent Innovations in DRAM Manufacturing. *2010 21st Annual IEEE/SEMI Advanced Semiconductor Manufacturing Conference (ASMC)* **2010**, 264−269.

(5) Kiguchi, T.; Nakamura, S.; Akama, A.; Shiraishi, T.; Konno, T. J. Solid State Epitaxy of $(Hf,Zr)O_2$ Thin Films with Orthorhombic Phase. *J. Ceram. Soc. Jpn.* **2016**, *124*, 689−693.

(6) Fan, Z.; Xiao, J.; Wang, J.; Zhang, L.; Deng, J.; Liu, Z.; Dong, Z.; Wang, J.; Chen, J. Ferroelectricity and Ferroelectric Resistive Switching in Sputtered $Hf_{0.5}Zr_{0.5}O_2$ Thin Films. *Appl. Phys. Lett.* **2016**, *108*, 232905.

(7) Ambriz-Vargas, F.; Kolhatkar, G.; Broyer, M.; Hadj-Youssef, A.; Nouar, R.; Sarkissian, A.; Thomas, R.; Gomez-Yáñez, C.; Gauthier, M. A.; Ruediger, A. A Complementary Metal Oxide Semiconductor Process-Compatible Ferroelectric Tunnel Junction. *ACS Appl. Mater. Interfaces* **2017**, *9*, 13262−13268.

(8) Lee, Y. H.; Kim, H. J.; Moon, T.; Kim, K. D.; Hyun, S. D.; Park, H. W.; Lee, Y. B.; Park, M. H.; Hwang, C. S. Preparation and Characterization of Ferroelectric $Hf_{0.5}Zr_{0.5}O_2$ Thin Films Grown by Reactive Sputtering. *Nanotechnology* **2017**, *28*, 305703.

(9) Das, K.; Tripathy, N.; Ghosh, S.; Sharma, P.; Singhal, R.; Kar, J. Microstructural, Surface and Interface Properties of Zirconium Doped HfO_2 Thin Films Grown by RF Co-sputtering Technique. *Vacuum* **2017**, *143*, 288−293.

(10) Ambriz-Vargas, F.; Kolhatkar, G.; Thomas, R.; Nouar, R.; Sarkissian, A.; Gomez Yáñez, C.; Gauthier, M. A.; Ruediger, A. Tunneling Electroresistance Effect in a $Pt/Hf_{0.5}Zr_{0.5}O_2/Pt$ Structure. *Appl. Phys. Lett.* **2017**, *110*, No. 093106.

(11) Migita, S.; Ota, H.; Yamada, H.; Shibuya, K.; Sawa, A.; Toriumi, A. Polarization Switching Behavior of Hf Zr O Ferroelectric Ultrathin films Studied Through Coer cive Field Characteristics. *Jpn. J. Appl. Phys.* **2018**, *57*, No. 04FB01.

(12) Bouaziz, J.; Rojo Romeo, P.; Baboux, N.; Vilquin, B. Characterization of Ferroelectric Hafnium/Zirconium Oxide Solid Solutions Deposited by Reactive Magnetron Sputtering. *J. Vac. Sci. Technol., B: Nanotechnol. Microelectron.: Mater., Process., Meas., Phenom.* **2019**, *37*, No. 021203.

(13) Migita, S.; Ota, H.; Shibuya, K.; Yamada, H.; Sawa, A.; Matsukawa, T.; Toriumi, A. Phase Transformation Behavior of Ultrathin $Hf_{0.5}Zr_{0.5}O_2$ Films Investigated Through Wide Range Annealing Experiments. *Jpn. J. Appl. Phys.* **2019**, *58*, SBBA07.

(14) Luo, Q.; Ma, H.; Su, H.; Xue, K.-H.; Cao, R.; Gao, Z.; Yu, J.; Gong, T.; Xu, X.; Yin, J.; Yuan, P.; Tai, L.; Dong, D.; Long, S.; Liu, Q.; Miao, X.-S.; Lv, H.; Liu, M. Composition-Dependent Ferroelectric Properties in Sputtered $Hf_XZr_{1-X}O_2$ Thin Films. *IEEE Electron Device Lett.* **2019**, *40*, 570−573.

DOI: 10.1021/acsaelm.9b00367
ACS Appl. Electron. Mater. XXXX, XXX, XXX−XXX

(15) Zhou, D.; Xu, J.; Li, Q.; Guan, Y.; Cao, F.; Dong, X.; Müller, J.; Schenk, T.; Schröder, U. Wake-up Effects in Si-doped Hafnium Oxide Ferroelectric Thin Films. *Appl. Phys. Lett.* **2013**, *103*, 192904.
(16) Starschich, S.; Menzel, S.; Böttger, U. Pulse Wake-up and Breakdown Investigation of Ferroelectric Yttrium doped HfO_2. *J. Appl. Phys.* **2017**, *121*, 154102.
(17) Starschich, S.; Menzel, S.; Böttger, U. Evidence for Oxygen Vacancies Movement During Wake-up in Ferroelectric Hafnium Oxide. *Appl. Phys. Lett.* **2016**, *108*, 032903.
(18) Fengler, F. P.; Hoffmann, M.; Slesazeck, S.; Mikolajick, T.; Schroeder, U. On The Relationship Between Field Cycling and Imprint In Ferroelectric $Hf_{0.5}Zr_{0.5}O_2$. *J. Appl. Phys.* **2018**, *123*, 204101.
(19) Grimley, E. D.; Schenk, T.; Sang, X.; Pešić, M.; Schroeder, U.; Mikolajick, T.; LeBeau, J. M. Structural Changes Underlying Field-Cycling Phenomena in Ferroelec tric HfO_2 Thin Films. *Advanced Electronic Materials* **2016**, *2*, 1600173.
(20) Park, M. H.; Kim, H. J.; Kim, Y. J.; Jeon, W.; Moon, T.; Hwang, C. S. Ferroelectric Properties and Switching Endurance of $Hf_{0.5}Zr_{0.5}O_2$ Films on TiN Bottom and TiN or RuO_2 Top Electrodes. physica status solidi (RRL). *Phys. Status Solidi RRL* **2014**, *8*, 532−535.
(21) Hyuk Park, M.; Joon Kim, H.; Jin Kim, Y.; Moon, T.; Seong Hwang, C. The Effects of Crystallographic Orientation and Strain of Thin $Hf_{0.5}Zr_{0.5}O_2$ Film on its Ferroelectricity. *Appl. Phys. Lett.* **2014**, *104*, No. 072901.
(22) Hyuk Park, M.; Joon Kim, H.; Jin Kim, Y.; Lee, W.; Kyeom Kim, H.; Seong Hwang, C. Effect of Forming Gas Annealing on the Ferroelectric Properties of $Hf_{0.5}Zr_{0.5}O_2$ Thin Films with and without Pt Electrodes. *Appl. Phys. Lett.* **2013**, *102*, 112914.
(23) Park, M. H.; Kim, H. J.; Kim, Y. J.; Lee, W.; Moon, T.; Kim, K. D.; Hwang, C. S. Study on the Degradation Mechanism of the Ferroelectric Properties of Thin $Hf0.5Zr_{0.5}O_2$ Films on TiN and Ir Electrodes. *Appl. Phys. Lett.* **2014**, *105*, 072902.
(24) Kim, S. J.; Narayan, D.; Lee, J.-G.; Mohan, J.; Lee, J. S.; Lee, J.; Kim, H. S.; Byun, Y. c.; Lucero, A. T.; Young, C. D.; Summerfelt, S. R.; San, T.; Colombo, L.; Kim, J. Large Ferroelectric Polarization of $TiN/Hf_{0.5}Zr0.5O_2/TiN$ Capacitors Due to Stress-induced Crystallization at Low Thermal Budget. *Appl. Phys. Lett.* **2017**, *111*, 242901.
(25) Chernikova, A. G.; Kozodaev, M. G.; Negrov, D. V.; Korostylev, E. V.; Park, M. H.; Schroeder, U.; Hwang, C. S.; Markeev, A. M. Improved Ferroelectric Switching Endurance of La-Doped $Hf_{0.5}Zr_{0.5}O_2$ Thin Films. *ACS Appl. Mater. Interfaces* **2018**, *10*, 2701−2708.

DOI: 10.1021/acsaelm.9b00367
ACS Appl. Electron. Mater. XXXX, XXX, XXX−XXX